DEFENSE TECHNICAL INFORMATION CENTER

Information for the Defense Community

DTIC® has determined on 10/05/2012 that this Technical Document has the Distribution Statement checked below. The current distribution for this document can be found in the DTIC® Technical Report Database.

☒ **DISTRIBUTION STATEMENT A.** Approved for public release; distribution is unlimited.

☐ **© COPYRIGHTED**; U.S. Government or Federal Rights License. All other rights and uses except those permitted by copyright law are reserved by the copyright owner.

☐ **DISTRIBUTION STATEMENT B.** Distribution authorized to U.S. Government agencies only (fill in reason) (date of determination). Other requests for this document shall be referred to (insert controlling DoD office)

☐ **DISTRIBUTION STATEMENT C.** Distribution authorized to U.S. Government Agencies and their contractors (fill in reason) (date of determination). Other requests for this document shall be referred to (insert controlling DoD office)

☐ **DISTRIBUTION STATEMENT D.** Distribution authorized to the Department of Defense and U.S. DoD contractors only (fill in reason) (date of determination). Other requests shall be referred to (insert controlling DoD office).

☐ **DISTRIBUTION STATEMENT E.** Distribution authorized to DoD Components only (fill in reason) (date of determination). Other requests shall be referred to (insert controlling DoD office).

☐ **DISTRIBUTION STATEMENT F.** Further dissemination only as directed by (inserting controlling DoD office) (date of determination) or higher DoD authority.

Distribution Statement F is also used when a document does not contain a distribution statement and no distribution statement can be determined.

☐ **DISTRIBUTION STATEMENT X.** Distribution authorized to U.S. Government Agencies and private individuals or enterprises eligible to obtain export-controlled technical data in accordance with DoDD 5230.25; (date of determination). DoD Controlling Office is (insert controlling DoD office).

The Coupling of Gravity Waves and Turbulence at White Sands, New Mexico, from VHF Radar Observations

G. D. NASTROM

F. D. EATON

Reprinted from JOURNAL OF APPLIED METEOROLOGY, Vol. 32, No. 1, January 1993
American Meteorological Society

Reprinted from JOURNAL OF APPLIED METEOROLOGY, Vol. 32, No. 1, January 1993
American Meteorological Society

The Coupling of Gravity Waves and Turbulence at White Sands, New Mexico, from VHF Radar Observations

G. D. NASTROM

ESC1 , *St. Cloud State University, St. Cloud, Minnesota* M.N. , 56301

F. D. EATON

U.S. Army Atmospheric Sciences Laboratory, White Sands Missile Range, New Mexico

(Manuscript received 3 February 1992, in final form 29 June 1992)

ABSTRACT

Doppler spectra taken with the VHF Doppler radar at White Sands Missile Range are used to describe the winds and turbulence for 10 days in March–April 1991. The large power aperture product of this radar provides excellent data coverage in 150-m layers over the entire height range used, about 5–20 km. The results show that gravity-wave activity and small-scale turbulence are significantly enhanced at all levels during times when wind speeds in the troposphere, near 5.6 km (about 500 hPa), are strong. Largest enhancements are found in the lower stratosphere, near 16–18 km, where the mean $\log C_n^2$ is increased by over 10 dB during times of strong winds at low levels. Mean winds, wind shears, and static stability in the lower stratosphere were found to be nearly the same, regardless of wind speeds at low levels. The authors conclude that the enhanced turbulence is due to an effect not described by the local background wind and static stability, and suggest that this effect is upward-propagating gravity waves launched in the troposphere during the periods of strong winds.

1. Introduction

Small-scale turbulence in the atmosphere plays an important role in a variety of processes, including the effects of the atmosphere on the propagation of electromagnetic waves. Atmospheric effects on electromagnetic waves are often paramcterized by the refractivity turbulence structure constant C_n^2. Direct measurements of C_n^2 are relatively rare, and most of the available data coverage is limited in time and space or has poor resolution. Thus, there have been several efforts to infer or model C_n^2 as a function of the more widely available variables based on the background flow.

Hufnagel (1974) used observations of C_n^2 from a variety of sources to derive a simple model of its variability in terms of the strength of the horizontal winds aloft. VanZandt et al. (1978) and Warnock and VanZandt (1985) used vertical profiles of C_n^2 observed by a stratosphere–troposphere (ST) radar (also called a wind profiler radar) to calibrate a stochastic model of C_n^2. In their model, a spectrum of gravity waves is presumed to act upon the background profiles of wind and temperature, causing the Richardson number to fall below a threshold value (0.25) in small regions and giving rise to turbulence. More recently, Fairall et al. (1991) have refined the VanZandt and Warnock model to include a saturated spectrum of gravity waves and have incorporated the gravity-wave model of Sidi et al. (1988).

While this evolutionary improvement in our ability to model C_n^2 and its variability is encouraging, some features of the variability and of its coupling to the background flow remain only poorly described or understood. For example, Fairall et al. (1991) noted that the total wave energy density is a free paramcter in the Sidi et al. (1988) model and that Jasperson et al. (1990) give evidence suggesting that it varies with timc and location. Further, Warnock et al. (1989) found large differences in the gravity-wavc amplitudes needed to model C_n^2 observations in Colorado compared to those used in Illinois. No study, however, has yet sought to describe how C_n^2 differs in rcgions near wavc sourccs compared to nonsource regions. The purpose of this paper is to prcsent rcsults that show that under certain conditions the values of C_n^2 in the lower stratosphere vary by up to an order of magnitude, depending on the gravity-wave source conditions in the lower atmosphere. The differences apparently depend only on conditions in the lower atmosphere as they are found despite the presence of similar background stability and wind-shear conditions in the lower stratosphcrc.

The paper is organized as follows. Section 2 describes the radar system and cites the specific data period used

Corresponding author address: Dr. G. D. Nastrom, Department of Earth Sciences, St. Cloud State University, 720 Fourth Avenue South, St. Cloud, MN 56301-4498.

here. Section 3 presents the comparison of C_n^2 values and background flow conditions. Section 4 contains a summary and our conclusions.

2. VHF radar system

The radar used in this study is located at 32°24′N, 106°21′W, at 1220 m MSL; about 13 km east of the post area at White Sands Missile Range (WSMR), New Mexico. This site is in the Tularosa basin about 25 km east of the Organ Mountains. The immediate local area is characterized by flat terrain covered with low brush.

Salient parameters of the WSMR VHF radar are given in Table 1. The radar operates at 49.25 MHz, with fixed coaxial–collinear antennas at right angles. Beams are directed 15° from the zenith toward the east and north, and one is vertical, permitting the three components of the wind vector to be resolved. The antenna is about 150 m in diameter and produces a one-way beamwidth of 2.9°. Received power, from which C_n^2, wind speed, and spectral width are derived, is observed for 1 min along each beam. Since the three different beams are sampled consecutively, a full profile is obtained every 3 min. Pulse coding applied to the 8-μs transmitted pulses produces 1-μs nominal pulse lengths to give 150-m resolution along each beam axis. In normal operation, 112 range gates are used to sample from 3.22 to 20 km in altitude.

TABLE 1. Radar parameters used in this study.

Transmitter	
Nominal frequency	49.25 MHz
Output power	250-kW peak
Duty cycle	5%
Pulse width (compressed)	8 μs (8:1) 1 μs nominal
Type	combination solid-state preamplifier and tube-cavity amplifier, three stage
Antenna	
Physical aperture	15 600 m^2
Effective aperture	13 500 m^2
Pointing	Zenith and 15° to north and east
Type	phased array of coaxial collinear elements
One-way beamwidth	2.9°
Receiver	
Type	low-noise superheterodyne
Bandwidth	matched to transmitted pulse
Receiver noise figure	less than 1 dB
Performance	
Nominal lowest range gate	2 km above ground level
Range-gate spacing	150 m
Time resolution	1 min per beam
Number of range gates	112
Horizontal wind range	± 116 m s^{-1}
Calibrated C_n^2 range	10^{-20}–10^{-13} m$^{-2/3}$
Bandwidth	1 MHz
Power aperture product	1×10^8 W m^2

The transmitted peak power is 250 kW and leads to a power aperture product of 1×10^8 W m^2. Consequently, the signal-to-noise ratio is high at all levels sampled. In fact, the large transmitted energy often leads to sidelobe problems that give double peaks in the Doppler spectrum at the lower heights, making velocity measurements uncertain at low altitudes. This problem was found below about 5 km in the oblique beams and below about 7 km in the vertical beam. At higher altitudes, checks of the time and space continuity of the winds were used to help eliminate spurious points. The radar was calibrated for calculations of C_n^2 by comparing the returned signal with a signal of known strength; nevertheless, small differences exist between the radar systems in the east and north beams. We found it necessary to increase mean C_n^2 values in the east beam by 2 dB to match the mean values in the north beam.

The radar has been operated in a campaign mode in its early period of use. In this paper we use data from a time when observations were taken nearly continuously over an extended period. Specifically, data were taken from 0000 UTC 29 March 1991 through 2100 UTC 4 April 1991 and 1600 UTC 8 April 1991 through 1200 UTC 10 April 1991.

3. Results

Hourly mean horizontal wind vectors are shown in Fig. 1a for the first week of the period of observations used here. For clarity, only every fifth level is plotted. The associated hourly standard deviations, plotted in a vector format, are shown in Fig. 1b. Occasional outliers are noted in Fig. 1b, such as near 8 km on 1 April, and these were later eliminated from the data by hand editing.

The period used here was a time of rich synoptic weather variability. Surface cold fronts passed White Sands at 0300 UTC 30 March 1991 and 0600 UTC 2 April 1991, and a strong surface trough passed at about 0600 UTC 4 April 1991. The operational weather map analyses at 500 hPa show that troughs passed about 1200 UTC 30 March 1991, 1200 UTC 2 April 1991, and 1200 UTC 4 April 1991, and that ridge axes passed about 0000 UTC 1 April 1991 and 1200 UTC 3 April 1991. The flow changes associated with the passage of each of these features are clearly seen in the time series at 6 km in Fig. 1a; for example, the winds rapidly veer from westerly or southwesterly to northwesterly after the trough passages.

The standard deviations of the horizontal winds appear to be enhanced at all levels below about 19 km during the trough passages on 30 March, 2 April, and 4 April. Also, the standard deviations of the vertical velocities are increased at all levels during these times (Fig. 2). We follow Ecklund et al. (1982) in using the variance of the vertical velocity as an indicator of gravity-wave activity. The results in Figs. 1b and 2, with

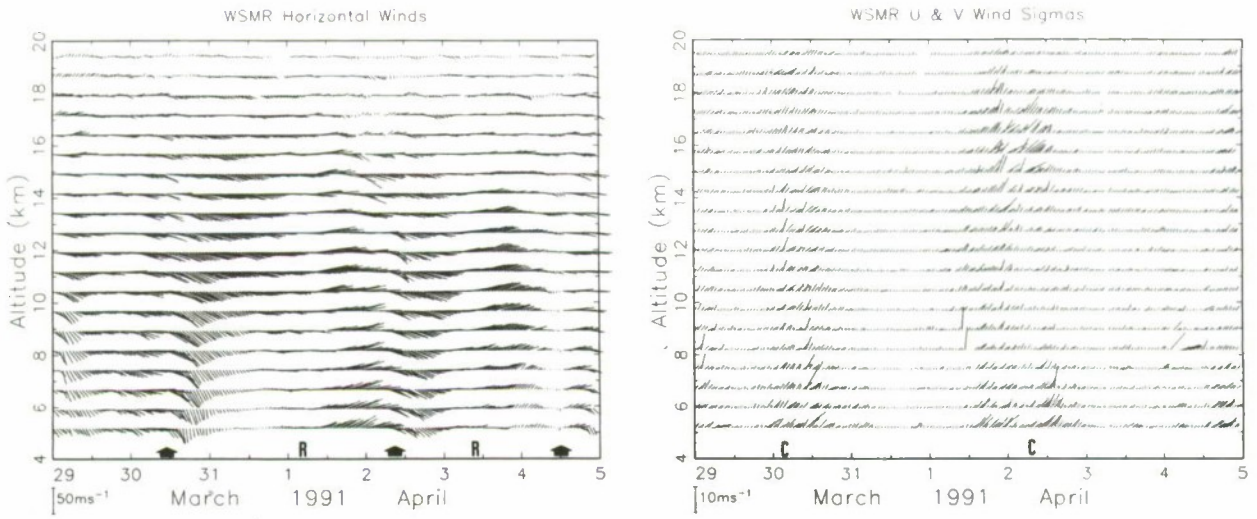

FIG. 1. Time series of (a) hourly mean horizontal winds at White Sands, plotted in vector format with north at the top and speed proportional to length. Approximate times of trough (ridge) passages at 500 hPa (about 5.6 km) are indicated by arrows (R's) along the abscissa. (b) Hourly standard deviations of horizontal winds, times of cold-front passages at the surface are indicated by C's.

enhanced activity at all heights during the trough passages, suggest that the source of the gravity waves is in the lower troposphere. Sato (1990) gives evidence that the similar periods of enhanced activity seen in the vertical velocity time series at the MU radar in Japan are due to flow over rough terrain. On the other hand, Nastrom et al. (1990) found that increased activity over the Flatland radar in Illinois was associated with low stability in the planetary boundary layer. Since the times of trough passage seen here are accompanied by both strong winds near local mountaintop heights and by low stability associated with surface fronts, the mechanism responsible for the gravity waves cannot be specified. In any case, however, a good indicator of enhanced gravity-wave activity appears to be increased tropospheric wind speed. This coupling is established by the correlation coefficients in Fig. 3, which show that the highest correlation of the variance of vertical velocity at all heights is with the wind speed in the troposphere below about 9 km.

To illustrate further the coupling of wind-speed changes in the middle troposphere and gravity-wave activity and turbulence at all heights, we sorted the hourly mean values according to the wind speed at 5.6

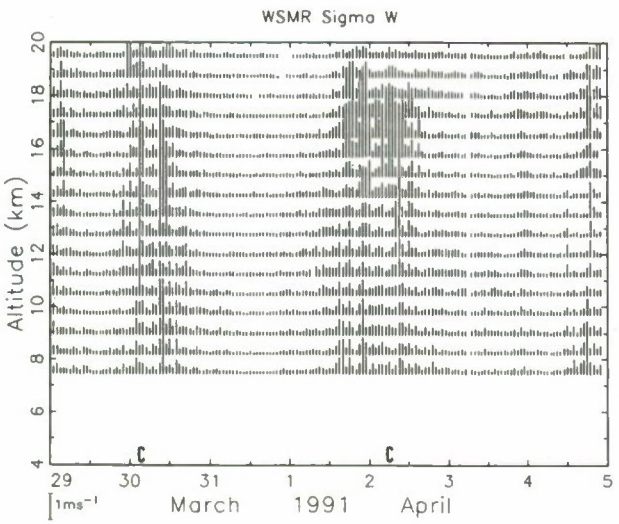

FIG. 2. Time series of hourly standard deviations of vertical velocity at White Sands. Low signal-to-noise ratios were found below 7 km due to electronic effects. Times of cold-front passages at the surface are indicated by C's.

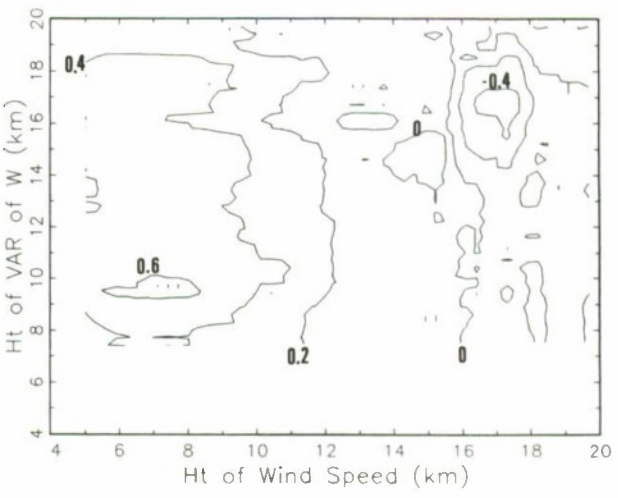

FIG. 3. Correlations between hourly variance of the vertical velocities at the height given on the ordinate with the hourly mean wind speeds at the height given on the abscissa. Note that there is relatively large positive correlation of var(W) at all heights, with wind speeds below about 10 km.

km (about 500 hPa) and then compared average values from the upper tercile (greater than 22 m s^{-1}) and lower tercile (less than 11 m s^{-1}). We find that the mean variance of vertical velocity (Fig. 4) is about three times greater in the troposphere during periods of strong winds compared to periods of weak winds. The enhancement during strong winds is up to a factor of 13 near 16 km, and decreases above 17 km to a factor of about 2 at 20 km.

The gradual growth of wave amplitude seen in Fig. 4 from about 10 to 15 km can be explained by the need for upward-propagating waves to conserve specific energy despite the decrease of density with height. The rate of growth of amplitude from 15 to 16 km, however, is too rapid to be due to decreases in density, and it implies that an instability must occur in the wave field. Further, the rapid decrease of wave amplitude above 17 km implies that energy has been removed from the upward-propagating gravity waves. These features suggest that wave-amplitude growth during upward propagation leads to wave instability and turbulent wave breaking. We note that Lilly and Kennedy (1973) and Danielsen and Mohnen (1977) also observed turbulent layers above growing waves near 16 km in aircraft experiments.

We will test the suggestion that the decrease in vertical velocity variance above 17 km is due to wave breaking in two ways. First, we will show that indicators of small-scale turbulence are also greatly enhanced near 17 km, thus supporting the notion of turbulent breakdown of the waves. Second, we will show that the profiles of the mean wind and stability are nearly the same in the stratosphere regardless of wind speed at 5.6 km and that the mean shear of the horizontal wind across layers only 300 m deep is also nearly the same, thus supporting the notion that the increased turbulence is due to a process other than instability of the background flow in the stratosphere.

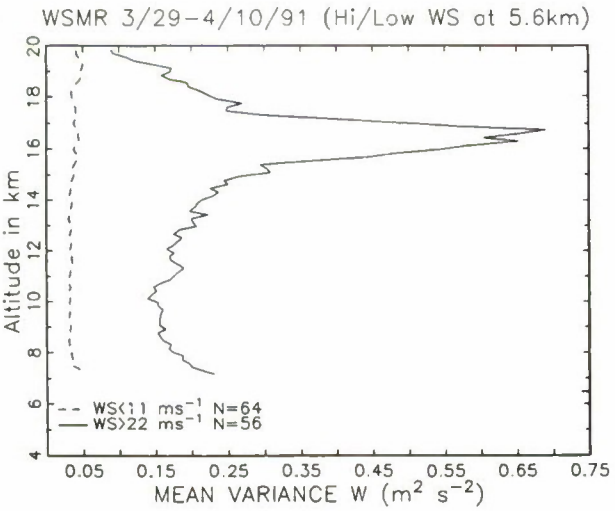

FIG. 4. Vertical profiles of the mean hourly variance of vertical velocity with hours sorted according to the wind speed at 5.6 km. Means for the upper and lower terciles are plotted.

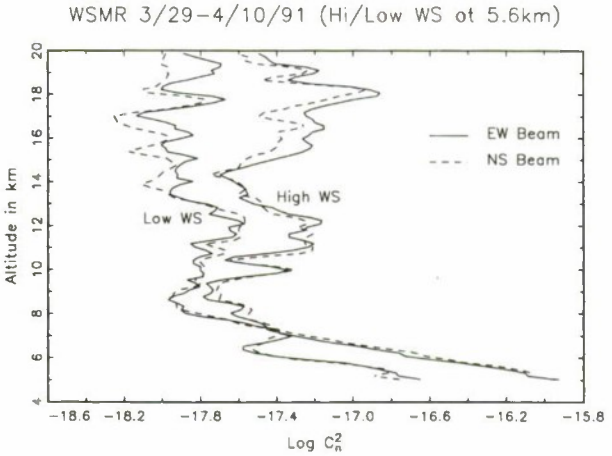

FIG. 5. As in Fig. 4 except for means of logC_n^2.

Figure 5 shows the mean profiles of the logarithm of C_n^2 for hours of high and low wind speed at 5.6 km. Mean values are larger at all heights during high wind speeds compared to low wind speeds, and the increases range from about 7 dB below 6 km to about 10 dB in the stratosphere. The value of C_n^2 depends on the potential refractivity and on the intensity of turbulence within the scattering volume (e.g., VanZandt et al. 1978; Gage 1990). The increased values of C_n^2 in the lower troposphere, below about 7 km, are likely due to enhanced potential refractivity from the increased moisture levels present during the passages of fronts and troughs that accompany high-wind conditions at 5.6 km. Increased values of C_n^2 at higher altitudes are likely due to increased turbulence rather than to a change in the potential refractivity (profiles of the stability index are shown later).

The spectral width (the second moment of the measured Doppler spectrum) is an indicator of small-scale turbulence not dependent on potential refractivity. It also increases by a factor of 2 or more in the stratosphere during times of high wind speeds at 5.6 km, as shown in Fig. 6. Gossard and Strauch (1983) identified several factors that influence the spectral width. Among these factors are the scattering elements within the sensed pulse volume moving at different speeds, particle fall speeds, changes in wind components in the radial direction, antenna motion, and finite width of the beam. For the conditions of this study (a fixed, vertically pointed beam in nonprecipitating or clear air), the last factor is the greatest contributor to artificial broadening of the spectra width. When a radar beam is not infinitesimal, the radial direction to the radar varies over the beam with a resultant range of vertical velocities toward or away from the radar even with a wind that is constant in speed and direction. The variance contribution is given by

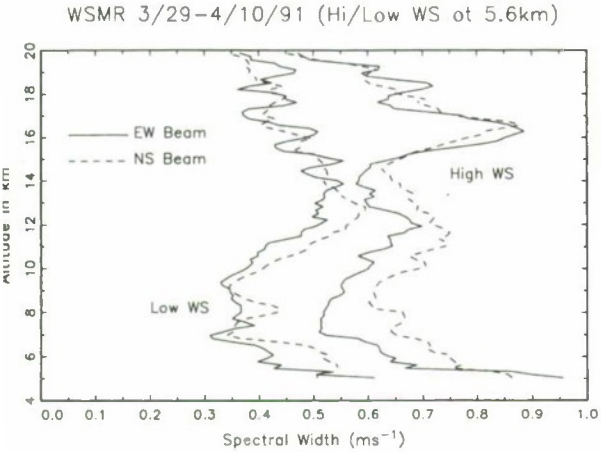

FIG. 6. As in Fig. 5 except for spectral width.

$$\sigma^2 = \frac{V_T^2 \Theta^2}{2.76}, \qquad (1)$$

where V_T is the component of the mean wind that is transverse to the beam axis and Θ is the half-width to the half-power (3 dB) point in the antenna pattern. Thus, the spectral width values shown in Fig. 6 are relatively correct in the 14–20-km range, since the mean winds are very similar in this range.

In summary, Figs. 4, 5, and 6 show that during high winds at 5.6 km the gravity-wave activity and the small-scale turbulence intensity are increased throughout the heights observed here. Largest relative increases are between 16 and 17 km. The wind and static stability of the background flow in this altitude region, however, are the same regardless of winds at 5.6 km, as shown next.

Figure 7 shows the vertical profiles of mean zonal and meridional wind speeds sorted according to the 5.6-km wind speed. For both components, mean speeds in the stratosphere are about the same regardless of the 5.6-km wind speed. Although the maximum speed is greater during high wind cases (Fig. 7), the nose of the jet stream is lower and the mean profiles are nearly identical above about 15 km. The mean meridional winds are slightly different in the troposphere, depending on the 5.6-km wind speed (southward during strong wind conditions and about zero near 6 km during weak-wind conditions), but are very similar in the stratosphere.

The mean vertical shears of the wind components are about the same regardless of wind speed at 5.6 km (Fig. 8). The mean shears were computed as follows: the absolute difference of the wind speeds in each component at each level for each individual observation was determined. Hourly averages of these individual differences were formed, and then the hourly averages were averaged after sorting them according to the hourly mean wind speed at 5.6 km. The mean shear

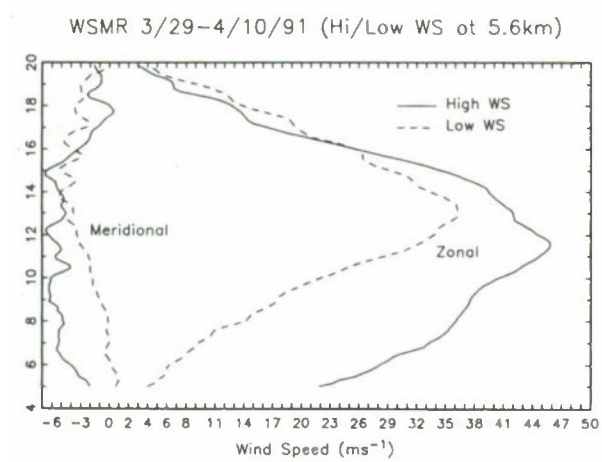

FIG. 7. As in Fig. 5 except for mean zonal and meridional wind speeds.

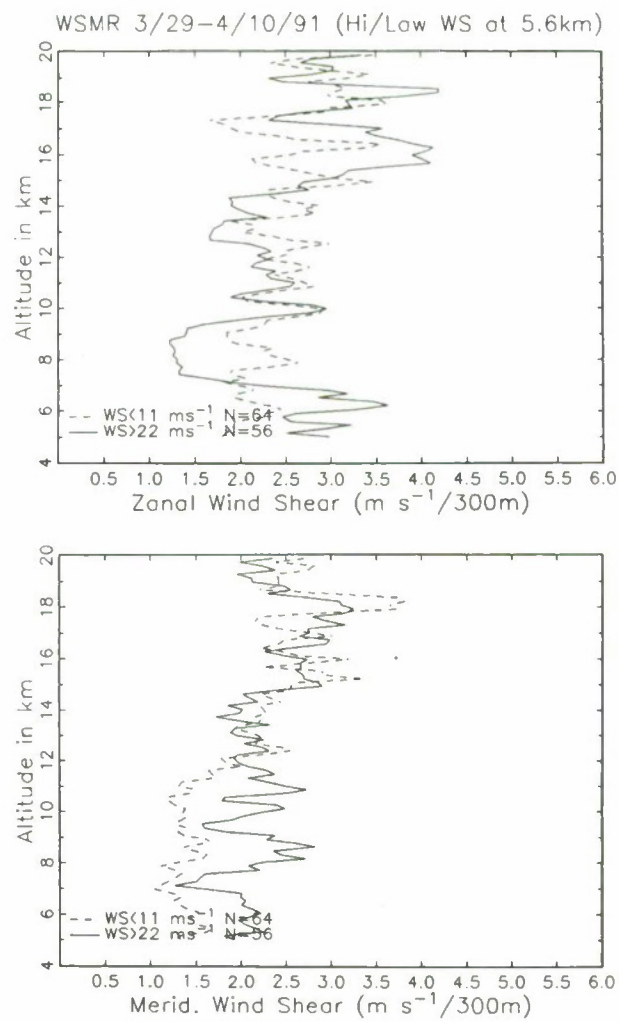

FIG. 8. As in Fig. 4 except for the mean shear of zonal and meridional wind speeds across 300-m layers.

values are near 3 m s^{-1} over 300-m layers in both u and v. Shears over 300-m layers, rather than 150-m layers, are used to avoid finite-range volume effects (Fukao et al. 1988). Since the basic data are at 3-min intervals, no attempt was made to correct the oblique velocities for the influences of vertical velocity, such as done by Strauch et al. (1987) for hourly values. The effects of vertical velocities on "shears" determined from oblique winds can be estimated by considering the differences of vertical velocity across 300-m layers. The median standard deviation of the vertical-wind-speed differences across 300-m layers during this period is about 0.2 m s^{-1} in the troposphere and 0.33 m s^{-1} in the stratosphere (increasing proportionally to the change in the Brunt–Väisälä frequency, as expected). These vertical wind differences would lead to apparent horizontal wind differences for measurements made on oblique beams of about 0.75 m s^{-1} in the troposphere and 1.2 m s^{-1} in the stratosphere. Such values are over a factor of 2 less than the mean horizontal wind shears observed in Fig. 8, suggesting that the results in Fig. 8 are not severely contaminated by vertical motions.

Finally, we note that the static stability of the lower stratosphere is about the same regardless of wind speed at 5.6 km. Figure 9 shows histograms of the Brunt–

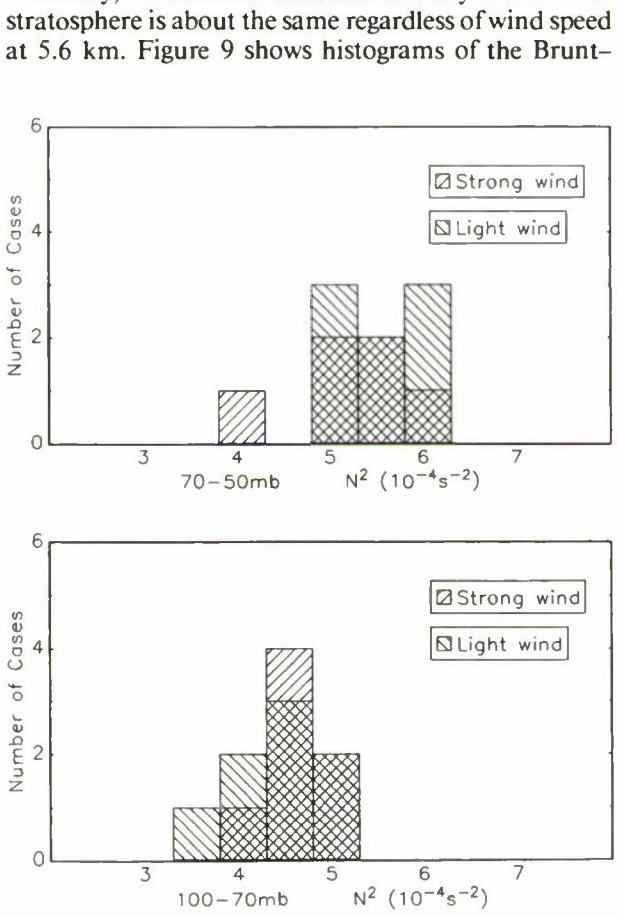

FIG. 9. Histograms of N^2 in two regions of the lower stratosphere, sorted according to whether horizontal winds at 5.6 km fell in the upper tercile (left hatch) or lower tercile (right hatch).

TABLE 2. Mean values of Brunt–Väisälä frequency squared (N^2, 10^{-4} s^{-2}) for high- and low-wind conditions.

Layer	High winds	Low winds
70–50 hPa	5.28	5.88
100–70	4.78	4.55
100–50	5.03	5.14
200–100	3.39	3.71
300–200	2.66	1.88
Number of cases	6	8

Väisälä frequency squared ($N^2 = g\partial \ln\theta/\partial z$) for the layers 100–70 hPa and 70–50 hPa. These values were estimated by using radiosonde data from the few balloons launched at WSMR plus those launched at El Paso, Texas, located about 60 km south of the radar site and available at 0000 and 1200 UTC daily. There is no apparent difference between the groups seen in Fig. 9. This result can be verified with the data in Table 2 by noting the similarity of the mean values in these levels and also at levels in the upper troposphere.

4. Conclusions

The White Sands 50-MHz radar was used to study high-resolution time and space variability of the mean winds and indicators of turbulence and gravity waves during a period in 1991. After meticulously editing the radar data by using space and time consistency checks to eliminate spurious signals produced by aircraft, etc. we performed a final check of the radar mean winds by comparing them with the synoptic weather patterns. During the period of data used here there were several episodes of strong winds in the troposphere, related to trough passages, with well-defined near-quiescent wind conditions between the trough passages. The radar mean winds display excellent agreement with the synoptic weather patterns.

The wind speed at 5.6 km (about 500 hPa) was used as an indicator of synoptic weather activity. During times of strong winds at 5.6 km (related to times of trough passages), the vertical velocity variance increases at all heights, with the largest increase approaching a factor of 13 in the stratosphere near 1 km. Refractivity turbulence C_n^2 and spectral width also show substantial increases at all heights during trough passage.

Apparently, the increased turbulence in the stratosphere during periods of strong winds at 5.6 km is due to the breaking of upward-propagating gravity waves that were launched by conditions in the lower troposphere associated with troughs (flow over rough terrain or decreased stability in the planetary boundary layer or both). This gravity-wave hypothesis is partly motivated by the observation that the mean vertical shear of the horizontal wind and the background static stability in the stratosphere are about the same regardless of lower-tropospheric wind speeds.

Past models of the refractivity turbulence structure constant C_n^2 have relied on variables associated with the background flow such as mean wind and temperature. The results of this study indicate that future models of refractivity turbulence should account for the strength of gravity-wave source mechanisms. [Preliminary comparisons of radar C_n^2 with results from the model of Warnock and VanZandt (1985) show large differences at about 16 km; these will be discussed in detail in a future paper.] Such mechanisms might be parameterized by using the background flow; for example, we have shown that the speed of the horizontal wind at 5.6 km is a good indicator of gravity-wave activity.

REFERENCES

Danielsen, E. F., and V. A. Mohnen, 1977: Project Dustorm report: Ozone transport, in situ measurements, and meteorological analyses of tropopause folding. *J. Geophys. Res.*, **37**, 5867–5877.

Ecklund, W. L., B. B. Balsley, R. G. Strauch, and J. L. Green, 1982: Vertical wind variability observed by VHF radar in the lee of the Colorado Rockies. *Mon. Wea. Rev.*, **110**, 1451–1457.

Fairall, C. W., A. B. White, and D. W. Thomson, 1991: A stochastic model of gravity-wave-induced clear-air turbulence. *J. Atmos. Sci.*, **48**, 1771–1790.

Fukao, S., T. Sato, T. Tsuda, S. Kato, M. Inaba, and I. Kimura, 1988: A systematic error in MST/ST radar measurement induced due to finite range volume effect: 1. Observational results. *Radio Sci.*, **23**, 59–73.

Hufnagel, R. E., 1974: Variations of atmospheric turbulence, in Digest of Technical Papers. *Topical Meeting on Optical Propagation Through Turbulence*, Optical Society of America, Washington, D.C., Wa 1-1–Wa 1-4.

Gage, K. S., 1990: Radar observations of the free atmosphere. *Radar in Meteorology*, David Atlas, Ed., Amer. Meteor. Soc., 534–565.

Gossard, E. E., and R. G. Strauch, 1983: *Radar Observations of Clear Air and Clouds*. Elsevier, 280 pp.

Jasperson, W. H., G. D. Nastrom, and D. C. Fritts, 1990: Further study of terrain effects on the mesoscale spectrum of atmospheric motions. *J. Atmos. Sci.*, **47**, 979–987.

Lilly, D. K., and P. J. Kennedy, 1973: Observations of a stationary mountain wave and its associated momentum flux and energy dissipation. *J. Atmos. Sci.*, **30**, 1135–1152.

Nastrom, G. D., M. R. Peterson, J. L. Green, and K. S. Gage, 1990: Sources of gravity waves as seen in the vertical velocity measured by the Flatland VHF radar. *J. Appl. Meteor.*, **29**, 783–792.

Sato, K., 1990: Vertical wind disturbances in the troposphere and lower stratosphere observed by the MU radar. *J. Atmos. Sci.*, **47**, 2803–2817.

Sidi, C., J. Lafrere, F. Dalaudier, and J. Barat, 1988: An improved atmospheric buoyancy wave spectrum model. *J. Geophys. Res.*, **93**, 774–790.

Strauch, R. G., B. L. Weber, A. S. Frisch, C. G. Little, D. A. Merritt, K. P. Moran, and D. C. Welsh, 1987: The precision and relative accuracy of profiler wind measurements. *J. Atmos. Oceanic Technol.*, **4**, 563–571.

VanZandt, T. E., J. L. Green, K. S. Gage, and W. L. Clark, 1978: Vertical profiles of refractivity turbulence structure constant: Comparison of observations by the Sunset radar with a new theoretical model. *Radio Sci.*, **13**, 819–829.

Warnock, J. M., and T. E. VanZandt, 1985: A statistical model to estimate the refractivity turbulence structure constant C_n^2 in the free atmosphere. NOAA TM ERL Al-10, 175 pp.

——, R. R. Beland, J. H. Brown, W. L. Clark, F. D. Eaton, L. D. Favier, K. S. Gage, J. L. Green, W. H. Hatch, J. R. Hines, E. A. Murphy, G. D. Nastrom, W. A. Peterson, T. E. VanZandt, 1989: Comparison among clear-air radar, thermosonde and optical measurements and model estimates of C_n^2 made in very flat terrain over Illinois. *Handbook for MAP*, Vol. 28, C. H. Liu and B. Edwards, Eds., 432–438. [Available from SCOSTEP Secretariat, University of Illinois, 1406 W. Green St., Urbana, IL 61801.]